Acta Crystallographica Section B
Structural Science
ISSN 0108-7681

Modulation functions of incommensurately modulated $Cr_2P_2O_7$ studied by the maximum entropy method (MEM)

Liang Li, Andreas Schönleber and Sander van Smaalen*

Laboratory of Crystallography, University of Bayreuth, 95440 Bayreuth, Germany

Correspondence e-mail: smash@uni-bayreuth.de

Received 27 August 2009
Accepted 27 January 2010

The maximum entropy method (MEM) has been used to determine electron density in superspace of incommensurately modulated chromium pyrophosphate from X-ray diffraction data measured by Palatinus *et al.* [(2006), *Acta Cryst.* B**62**, 556–566]. Chromium pyrophosphate, $Cr_2P_2O_7$, contains ordered regions (83% of the volume) and regions with disorder. Analysis of the MEM density has allowed the determination of the displacive modulation functions within ordered regions. The disordered regions can be described as the alternate occupation of two conformations of the pyrophosphate group and two positions of the chromium atom, with occupational probabilities that depend continuously on the phase of modulation t. A structure model based on the interpretation of the MEM density provides a fit to the diffraction data of the same quality as the model given by Palatinus *et al.* (2006). The failure to find a model that better fits the data is attributed to the intrinsic inaccuracy of ~ 0.01 Å for positions derived from the MEM and to the difficulties in constructing an appropriate model for the anharmonic ADPs and their modulation functions from electron densities.

1. Introduction

One of the applications of the maximum entropy method (MEM) in crystallography is the reconstruction of electron density from phased structure factors (Gilmore, 1996). Analysis of the MEM electron density can provide information about disorder (Dinnebier *et al.*, 1999; Wang *et al.*, 2001), anharmonic thermal motion (Kumazawa *et al.*, 1995; Bagautdinov *et al.*, 1998) and chemical bonding (Sakata & Sato, 1990; Takata, 2008; van Smaalen & Netzel, 2009). For aperiodic crystals the MEM has been used to determine the shapes of modulation functions of modulated crystals or the occupational domains of quasicrystals (Yamamoto *et al.*, 1996; Palatinus & van Smaalen, 2004; van Smaalen & Li, 2009).

The structures of incommensurately modulated crystals and composite crystals can be described as a periodic basic structure[1] combined with modulation functions for each of the independent atoms in the unit cell of the basic structure (van Smaalen, 2007; Janssen *et al.*, 2007). Structure models then incorporate for each independent atom three basic structure coordinates, atomic displacement parameters (ADPs) and, in principle, an infinite number of parameters defining the modulation functions for each independent atom. Since structure refinements can determine a finite number of parameters at best, modulation functions are usually described by truncated Fourier series. Often only the first harmonic or up to

[1] Composite crystals require two or more basic periods.

Table 1
Basic structural information as obtained from Palatinus *et al.* (2006).

The criterion for observed reflections is $I > 3\sigma(I)$.

Chemical formula	$Cr_2P_2O_7$
Superspace group	$C2/m(\sigma_1\,0\,\sigma_3)\bar{1}s$
a (Å)	7.0192 (5)
b (Å)	8.4063 (6)
c (Å)	4.6264 (3)
β (°)	108.6111 (64)
Modulation wavevector	[−0.361 (1), 0, 0.471 (1)]
$(\sin(\theta)/\lambda)_{max}$ (Å^{-1})	0.62
No. of reflections (obs/all)	1433/2409
No. of main reflections (obs/all)	278/283
No. of first-order satellites (obs/all)	455/495
No. of second-order satellites (obs/all)	421/569
No. of third-order satellites (obs/all)	183/495
No. of fourth-order satellites (obs/all)	96/567

second harmonics can be determined, while a larger number of parameters cannot be refined due to interdependences among them. Sometimes it appears appropriate to employ block waves or saw-tooth-shaped functions as modulation functions. However, in all cases the outcome of the structure refinements is restricted by the choice of parameters for the modulation functions. The result may differ from the true functions and it may not reflect the information content of the diffraction data.

The MEM has been proposed as a model-independent tool to obtain the most probable generalized electron density in the unit cell of superspace of aperiodic crystals. Analysis of the superspace density then provides a model-independent estimate of the modulation functions (van Smaalen *et al.*, 2003; van Smaalen, 2007). Several successful applications of this principle have been published (Palatinus & van Smaalen, 2004; McMahon *et al.*, 2007).

Chromium pyrophosphate, $Cr_2P_2O_7$, is a member of the thortveitite family of compounds (Glaum *et al.*, 1991). The thortveitite structure type is stable at high temperatures, while it defines the basic structure of the incommensurately modulated phase at room temperature (Table 1). The modulation becomes commensurate below T_c = 285 K. Structure refinements of $Cr_2P_2O_7$ have been performed by Palatinus *et al.* (2006), employing combinations of harmonic, block-wave and saw-tooth functions for the modulation functions. The analysis by Palatinus *et al.* (2006) showed small regions of large variations of the modulation functions that could not be properly described by a model. Here we present the results of an analysis by the MEM of the modulations in $Cr_2P_2O_7$ based on the X-ray diffraction data published by Palatinus *et al.* (2006). Although the structure model based on the MEM gives only a slightly better fit to the diffraction data, the analysis of the MEM density clearly reveals the way the structure resolves internal strain in the transition regions.

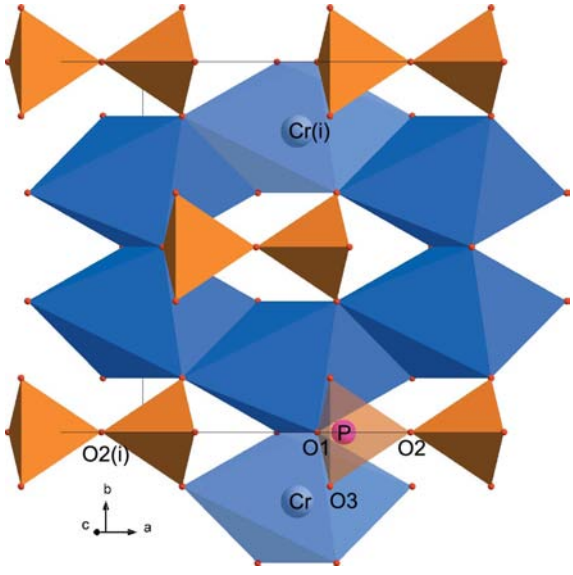

Figure 1
Basic structure of $Cr_2P_2O_7$. Cr(i) and O2(i) are related by lattice translations to Cr and O2, respectively.

The basic structure of $Cr_2P_2O_7$ is formed by layers of edge-sharing, distorted CrO_6 octahedra. Gaps in these layers are bridged by P_2O_7 pyrophosphate groups that share three of their O atoms with a layer below and three other O atoms with a layer above; the bridging O atom is confined to the P_2O_7 group (Fig. 1). The most probable origin for the incommensurability is that a fully relaxed (stretched) pyrophosphate group is larger than the gaps in the chromium oxide layers. The room-temperature crystal structure with the periodicity of the CrO_3 layers must thus contain the pyrophosphate group in an unfavorable conformation, which is relieved at low temperatures by forming an incommensurately modulated structure. Other contributions to the incommensurability could come from the Jahn–Teller distortions of the CrO_6 octahedral groups (Palatinus *et al.*, 2006).

2. The maximum entropy method

The generalized electron density $\rho_s(\mathbf{x}_s)$ in $(3+1)$-dimensional superspace is discretized on a grid of $N_{pix} = N_1 \times N_2 \times N_3 \times N_4$ pixels over the superspace unit cell. Then the entropy is defined as (van Smaalen *et al.*, 2003)

$$S = -\sum_{k=1}^{N_{pix}} \left(\rho_k \log\left[\rho_k/\rho_k^{prior}\right] - \rho_k + \rho_k^{prior}\right), \qquad (1)$$

where $\rho_k = \rho_s(\mathbf{x}_{sk})$ is the electron density at the kth grid point and ρ_k^{prior} is the corresponding value of the reference density or PRIOR. The MEM defines the optimal electron density as the electron density $\{\rho_k\}$ which maximizes the entropy S (1) subject to several constraints. The first constraint is the normalization of $\{\rho_k\}$ and $\{\rho_k^{prior}\}$

$$\frac{V}{N_{pix}} \sum_{k=1}^{N_{pix}} \rho_k = N_e, \qquad (2)$$

where N_e is the number of electrons in the unit cell and V is its volume. Diffraction data are incorporated in the form of the so-called F constraint, $C_{F^2} = 0$, with (Sakata & Sato, 1990)

Table 2
Comparison of MEM calculations with different weights.

R values at convergence as well as the number of reflections with $\Delta F/\sigma \geq 6$ and the value of $(\Delta F/\sigma)_{\max}$ are given.

	H0	H2	H4	F2	F4
R_F(all)	0.0392	0.0469	0.0450	0.0274	0.0245
wR_{F^2}(all)	0.0371	0.0372	0.0371	0.0373	0.0373
$\Delta F/\sigma \geq 6$	17	9	6	0	2
$(\Delta F/\sigma)_{\max}$	14.48	10.48	7.36	5.80	6.37

$$C_{F^2} = -1 + \frac{1}{N_F}\sum_{i=1}^{N_F} w_i \left(\frac{\left|F_{\rm obs}(\mathbf{H}_i) - F_{\rm MEM}(\mathbf{H}_i)\right|}{\sigma_i}\right)^2. \quad (3)$$

The sum runs over all independent structure factors N_F in the data set. $F_{\rm obs}(\mathbf{H}_i)$ is the phased observed structure factor of the reflection with scattering vector $\mathbf{H}_i$, and σ_i is the standard uncertainty of $|F_{\rm obs}(\mathbf{H}_i)|$. $F_{\rm MEM}(\mathbf{H}_i)$ is obtained by $(3+1)$-dimensional Fourier transform of the trial density $\{\rho_k\}$. The standard version of the MEM employs weights $w_i = 1$. The F constraint then represents χ^2 of the data with an expectation value of one. This value is achieved at convergence where $C_{F^2} = 0$.

For uncorrelated standard uncertainties σ_i one expects at convergence a normalized Gaussian distribution of the residuals

$$\frac{\Delta F(\mathbf{H}_i)}{\sigma_i} = \frac{F_{\rm obs}(\mathbf{H}_i) - F_{\rm MEM}(\mathbf{H}_i)}{\sigma_i}. \quad (4)$$

It has been shown that the MEM with $w_i = 1$ leads to distributions far from Gaussian in most cases. This feature is responsible for a converged density $\{\rho_k\}$ that is far from the optimum density $\{\rho_k^{\rm MEM}\}$ (de Vries *et al.*, 1994; Palatinus & van Smaalen, 2002).

Several weighting schemes have been proposed, which should guide the iterative MEM procedure towards the optimum density with a Gaussian distribution of residuals (4). A good choice for periodic crystals involves weights that vary according to an inverse power of the length of the scattering vector

$$w_i = \frac{1}{\left|\mathbf{H}_i\right|^n}\left(\frac{1}{N_F}\sum_{i=1}^{N_F}\frac{1}{\left|\mathbf{H}_i\right|^n}\right)^{-1} \quad (5)$$

with n a positive integer. These static weights are denoted by Hn. Optimal results have been obtained for weights H4 (de Vries *et al.*, 1994; Hofmann *et al.*, 2007).

An empirical justification for weights Hn is provided by the observation that a few low-order strong reflections attain large residuals. In this case $C_{F^2} = 0$ then implies that the other reflections will have too small values for their residuals (de Vries *et al.*, 1994). Strong reflections of periodic crystals have short scattering vectors and weights Hn define larger weights for exactly these reflections. In the case of incommensurately modulated crystals problematic reflections are again the strong reflections with short scattering vectors. However, reflections with short scattering vectors include both main reflections and satellite reflections. The latter are generally weak and they inadvertently obtain large weights, if weights of the type Hn are employed. Presently, we have found that weights H2 and H4 do not lead to optimal MEM densities, as indicated by the distributions of residuals (Table 2 and Fig. 2) and by the mismatch between modulation functions derived from the MEM densities and those of the model (Fig. 3).

Weights that emphasize the strong reflections can be alternatively chosen as weights proportional to some power of the structure-factor amplitude (de Vries *et al.*, 1994)

$$w_i = \left|F_{\rm obs}(\mathbf{H}_i)\right|^n \left(\frac{1}{N_F}\sum_{i=1}^{N_F}\left|F_{\rm obs}(\mathbf{H}_i)\right|^n\right)^{-1}. \quad (6)$$

These weights are denoted by Fn. Here we have found that an optimal result is obtained for weights F2. Although the distribution of residuals is not Gaussian for F2, this choice of weights gave the best performance for removal of the problem of very large residuals for a few reflections (Table 2). Another indication for the better performance of weights F2 is that they lead to a lower R_F value than weights Hn (Table 2).

Weights F2 are not necessarily the optimal choice for incommensurate crystals. One can envisage that other weighting schemes might work better or that different weighting schemes will appear optimal for different compounds. Nevertheless, weights F2 appear to give excellent results for $Cr_2P_2O_7$ (Fig. 3). Therefore, they have been used for the present analysis.

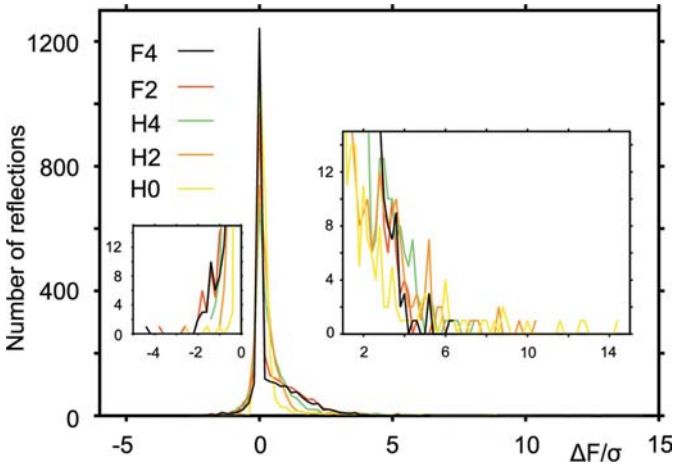

Figure 2
Distribution of residuals [see (4)] at convergence of the MEM for weights H0, H2, H4, F2 and F4. The inset shows an expanded view.

3. Experimental

3.1. Structure refinements

The present work is based on X-ray diffraction data by Palatinus *et al.* (2006). Properties of the data of particular relevance for the MEM are summarized in Table 1. Palatinus *et al.* (2006) present several models for the structure of incommensurately modulated $Cr_2P_2O_7$. Their model *A* is based on displacive modulation functions that are combina-

tions of saw-tooth, block-wave and harmonic functions. The atomic displacement parameters (ADPs) are modulated by harmonic functions in this model. Model *A* is characterized by discontinuities in the modulation functions at two values of *t* (Fig. 4).

Model *B* is proposed as their best model by Palatinus *et al.* (2006). It differs from model *A* as it contains regions of disordered structure around the *t* values which indicated discontinuities in model *A*. As a consequence, the modulation functions of the ADP could be removed from model *B*, resulting in fewer parameters and lower *R* values than in model *A*.

We have reproduced the refinement of model *B* employing the software *JANA*2006 (Petricek *et al.*, 2006). The disorder in model *B* is described by a split atom model of width 0.084 in *t*. The technical realisation involves the introduction of atoms Cr(*a*), P(*a*), P(*b*), O2(*a*), O3(*a*) and O3(*b*), each with an occupancy of one half and a width of 0.084 in *t*, while reducing the widths of the parent atoms by the same amount. The half-occupied atomic sites are not modulated in model *B*, because it is impossible to refine any occupational and displacive modulation parameters of these atoms due to high correlations caused by their small occupational domains in *t*. On the other hand, large structural variations exactly in the regions of disorder strongly suggest that these half-occupied sites will be modulated. Uncovering the crystal structure in the regions of disorder was one of the motivations for the use of the MEM for this system.

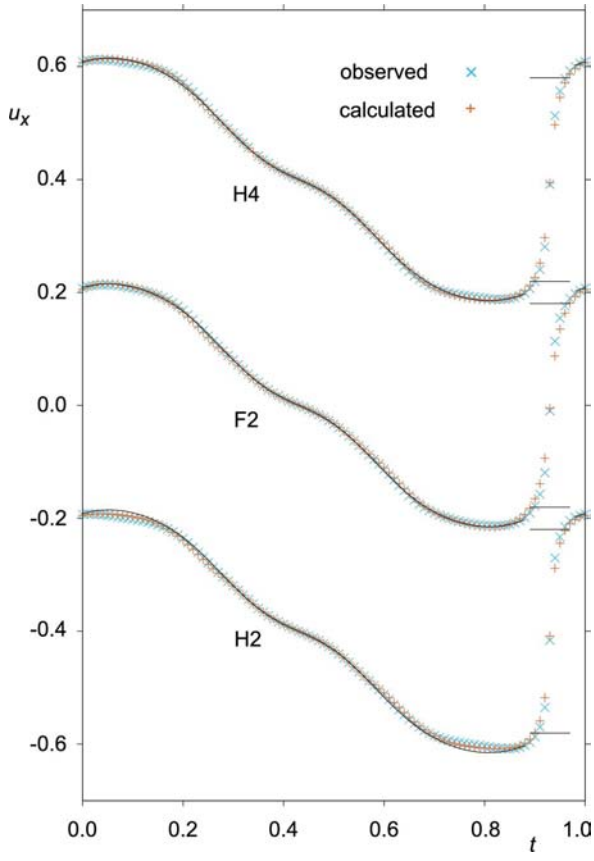

Figure 3
Modulation function u_x of Cr as obtained from MEM densities computed against observed data (×) and against F_{cal} as 'data' (+). Values obtained with weights H2, F2 and H4 are plotted with offsets of −0.4, 0 and 0.4 Å, respectively. The modulation function of refined model *B* is given as a solid line and reproduced at each offset value.

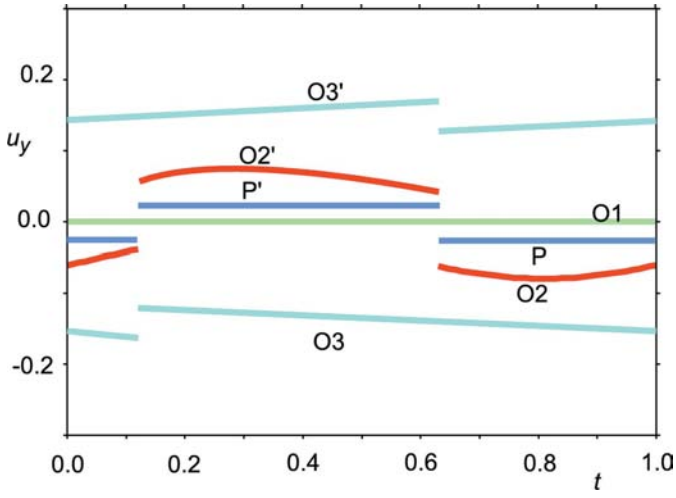

Figure 4
Schematic representation of the modulation functions in model *A*. The component u_y is shown as a function of *t*. Discontinuities are present at $t = 0.13$ and at $t = 0.63$. Primed atoms are related to unprimed atoms by the symmetry operator $(x_1, -x_2, x_3, \frac{1}{2} + x_4)$. Based on Fig. 4 of Palatinus *et al.* (2006).

Based on the analysis of the MEM density a new model has been developed, which provides an improved description of the structure although it gives only a marginally better fit to the data. This model, called model *M*, has been obtained by a real-space fit of the parameters of the modulation functions to the *t*-dependent positions of the atoms as they have been determined by interpretation of the MEM electron density (Fig. 5). Since these modulation functions are determined at one hundred *t* values, many more parameters can be fitted than is possible in structure refinements against diffraction data, thus obtaining a nearly perfect description of the *t*-dependent atomic positions as derived from the MEM density. As a consequence, only a selection of the structural parameters of model *M* could be refined against the diffraction data, while others have been kept fixed to their values determined from the MEM density. As discussed below, an improvement of the fit to the diffraction data was obtained just by replacing the displacive modulation of the P atom by MEM-derived functions. The modulation functions of the other atoms were kept as in model *B*. A summary of features of models *M* and *B* is given in Tables 3 and 4. Full details of models *M* and *B* are given as CIF files in the supplementary material.[2]

3.2. MEM calculations

The electron density has been defined on a grid of 72 × 96 × 48 × 48 pixels, which corresponds to a voxel size of

[2] Supplementary data for this paper are available from the IUCr electronic archives (Reference: BP5028). Services for accessing these data are described at the back of the journal.

Table 3
Number of parameters used for each atom in models *B* and *M*.

The number in brackets is the number of refined parameters.

	Model *B*			Model *M*			
	Occupancy	Position	Second ADP	Occupancy	Position	Second ADP	Third ADP
P	2 (0)	15 (15)	18 (18)	2 (0)	24 (3)	11 (11)	16 (16)
P(*a*)	2 (0)	3 (3)	6 (6)	6 (0)	24 (0)	6 (6)	0
P(*b*)	2 (0)	3 (3)	6 (6)	6 (0)	24 (0)	6 (6)	0
O2	2 (0)	4 (4)	4 (4)	2 (0)	4 (4)	4 (4)	0
O2(*a*)	2 (1)	3 (3)	6 (6)	2 (1)	3 (3)	6 (6)	0
O1	0	8 (8)	4 (4)	0	8 (8)	4 (4)	0
O3	2 (0)	24 (21)	18 (18)	2 (0)	24 (21)	18 (18)	0
O3(*a*)	2 (0)	3 (3)	6 (6)	2 (0)	3 (3)	6 (6)	0
O3(*b*)	2 (0)	3 (3)	6 (6)	2 (0)	3 (3)	6 (6)	0
Cr	2 (0)	16 (13)	16 (16)	2 (0)	16 (13)	16 (16)	0
Cr(*a*)	2 (1)	3 (3)	6 (6)	2 (1)	3 (3)	6 (6)	0

Table 4
R values and partial *R* values for model *B* and model *M*.

	Model *B*		Model *M*		No. of reflections	
Reflection group	R_F(obs)	wR_{F^2}(all)	R_F(obs)	wR_{F^2}(all)	Observed	All
All	0.0227	0.0577	0.0217	0.0568	1433	2409
Main	0.0165	0.0408	0.0157	0.0397	278	283
Satellites $\|m\| = 1$	0.0177	0.0308	0.0170	0.0294	455	495
Satellites $\|m\| = 2$	0.0330	0.0498	0.0317	0.0491	421	569
Satellites $\|m\| = 3$	0.0906	0.1822	0.0877	0.1779	183	495
Satellites $\|m\| = 4$	0.1962	0.3688	0.1846	0.3704	96	567
No. of parameters	179		170			

$0.097 \times 0.088 \times 0.096$ Å^3 in real space. Calculations according to the MEM have been performed with the software *BayMEM* on a Compaq-DEC ES40 Workstation (van Smaalen *et al.*, 2003). A uniform prior and the Cambridge algorithm have been used in all the calculations.

Observed, phased structure factors corrected for anomalous scattering have been generated from the diffraction data, employing model *B* according to the procedure described in Bagautdinov *et al.* (1998). They were used in one MEM calculation with weights F2 [see (6)], resulting in an optimized electron density $\rho^{\rm MEM}(\mathbf{x}_s) = \{\rho_k^{MEM}\}$. Additional MEM calculations have been performed with weights H0, H2, H4 and F4 (§2). Experimental values of phases are not available. Instead the MEM employs values for phases that are those of the best structure model. Therefore, they might differ from the true phases. For a centrosymmetric structure, like $Cr_2P_2O_7$, with two values, 0 or π, for the phase of each reflection, each phase can be correct or wrong. The use of difference-Fourier maps during structure solution depends on the fact that a partial, but reasonable, structure model already produces accurate reflection phases. For glycine we have counted 20 wrong phases out of 3822 reflections, of which only two (which were weak) possessed intensities larger than 3σ (Netzel *et al.*, 2008). True phases were assumed to be the values obtained from the multipole model. For $Cr_2P_2O_7$ we do not have an independent source of true phases, so we cannot make such an analysis in the present case.

Other MEM calculations have been performed with the combination of calculated structure factors of model *B* and experimental standard uncertainties as 'data'. Employing the

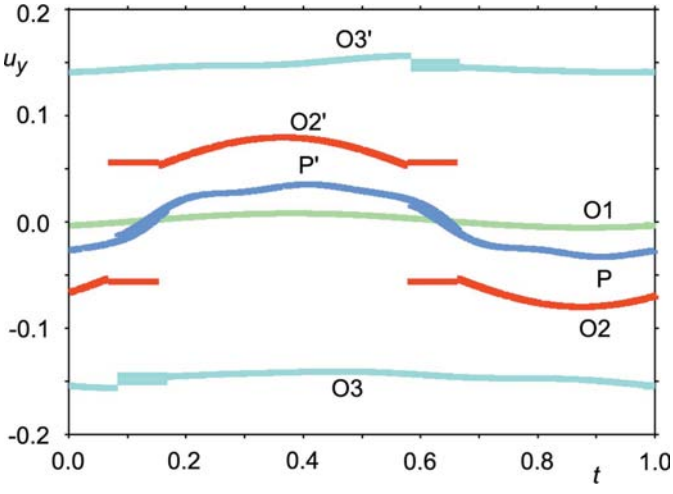

Figure 5
Schematic representation of the modulation functions in model *M*. The component u_y is shown as a function of *t*. Regions of disorder occur around $t = 0.12$ and $t = 0.62$.

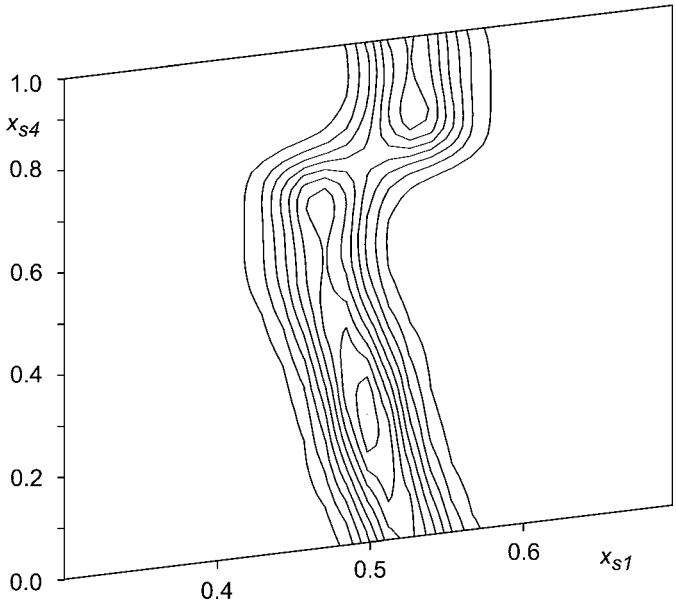

Figure 6
(x_{s1}, x_{s4})-Section of the generalized electron density $\rho_s^{\rm MEM}(\mathbf{x}_s)$ at the position Cr ($x_1 = 0.5$, $x_2 = 0.8121$ and $x_3 = 0.0$). The contour interval is 10% of the maximum electron density of 267.9 e Å^{-3}.

weight F2, the resulting density is denoted by $\rho_{\rm cal}^{\rm MEM}(\mathbf{x}_s) = \{\rho_{\rm cal,\,k}^{\rm MEM}\}$. Obviously, the latter calculation aims at reproducing the model, but differences with the model can occur due to the intrinsic behavior of the MEM, the choice of standard

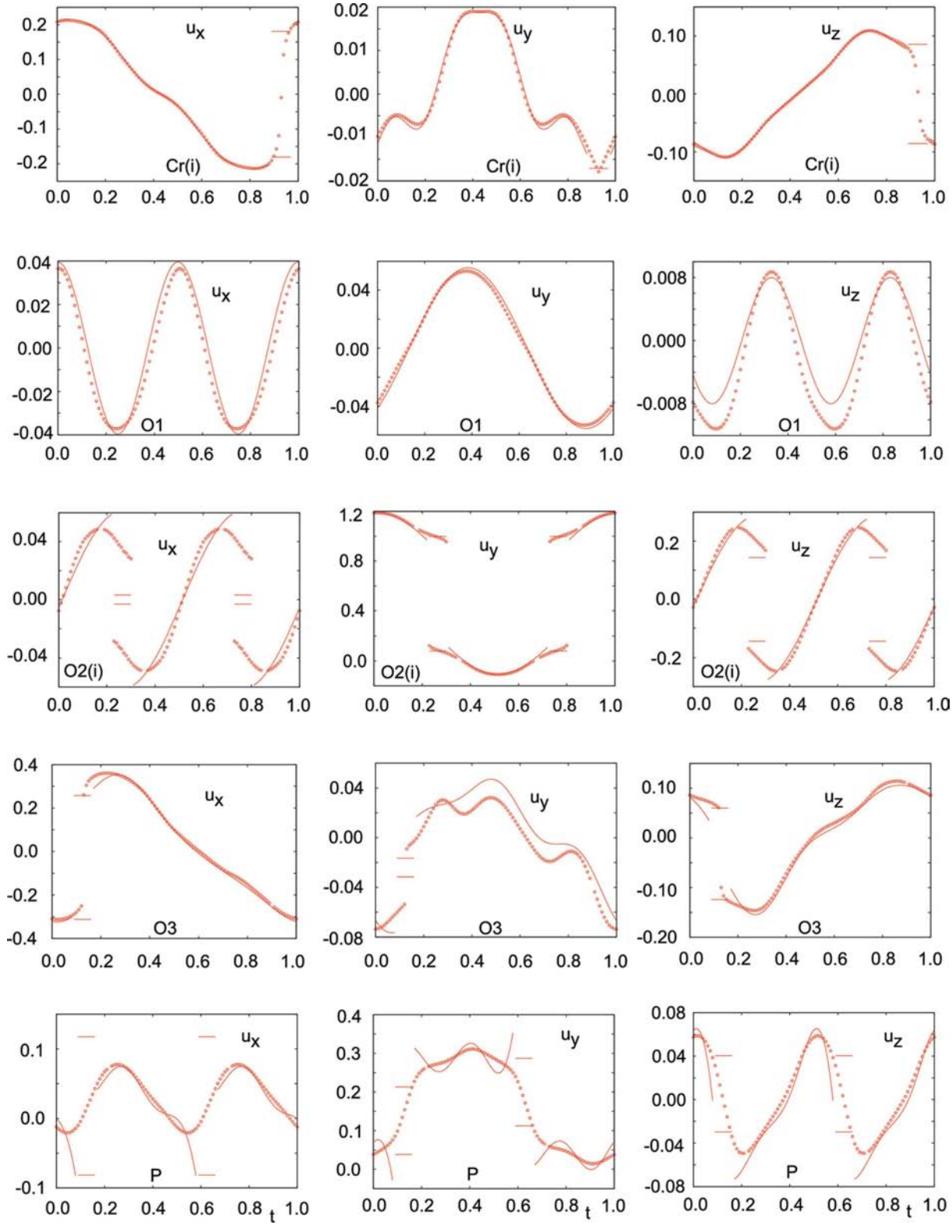

Figure 7
Modulation functions of the crystallographically independent atoms of $Cr_2P_2O_7$. Displacements along x, y and z are given in Å. Points are obtained from the MEM density; solid lines are the modulation functions of model *B*. Atoms are not necessarily bonded to each other as they are indicated in Fig. 1.

uncertainties and the limited number of reflections, which are restricted to those reflections for which experimental data are available.

The computer program *JANA*2006 (Petricek *et al.*, 2006) has been used for the visualization of two-dimensional sections of the electron densities. As an example, Fig. 6 gives the (x_{s1}, x_{s4}) section of $\rho^{\rm MEM}(\mathbf{x}_s)$ centered at the position of the Cr atom. It clearly shows the modulated position of this atom.

Electron-density maps have been quantitatively analyzed by the computer program *EDMA* (van Smaalen *et al.*, 2003). Three-dimensional sections representing physical space have been calculated from (3 + 1)-dimensional superspace densities for 100 equally spaced values of t with $0 \leq t < 1$. In each t section the positions of the atoms are identified as the local maxima of the density. Combining the information from all sections provides the positions of the atoms as functions of the modulation phase of t. The three components (u_x, u_y, u_z) of the modulation function of an atom then follow as the difference between its t-dependent position in the MEM density and its basic structure position obtained from model B. This procedure has been used, for example, to extract the modulation function of Cr from the MEM densities calculated with different weights (Fig. 3). The consideration of the modulations derived from $\rho^{\rm MEM}_{\rm cal}(\mathbf{x}_s)$ obtained with various weights shows that weights F2 provide the best convergence of the MEM (§2).

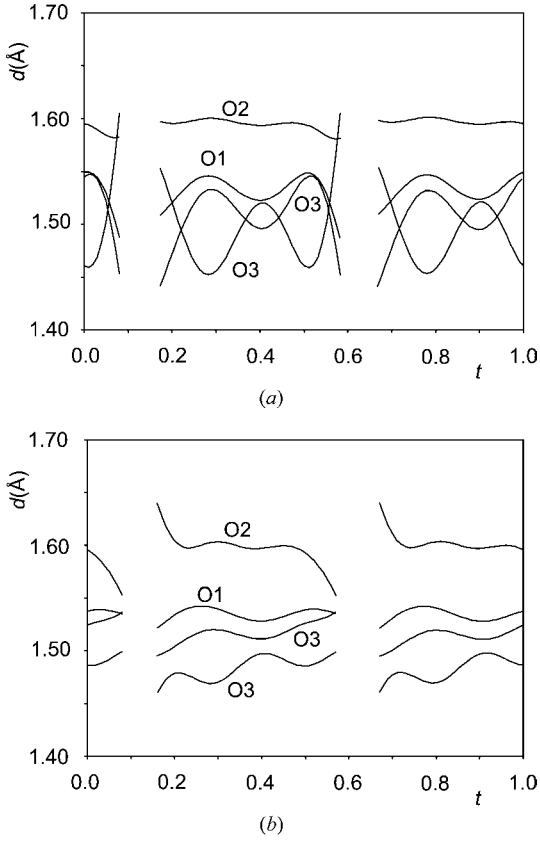

Figure 8
The coordination polyhedron of phosphorus depending on t. The disordered region is omitted. (*a*) P—O distances for model *B*. (*b*) P—O distances for model *M*.

Fig. 7 gives the modulation functions of all atoms: modulation functions from model *B* are compared with modulation functions as they have been determined from $\rho^{\rm MEM}(\mathbf{x}_s)$. The true position of an atom may deviate from the MEM-derived position by up to 0.01 Å for the grid size used in the present work (van Smaalen *et al.*, 2003). However, for atoms in special positions this discrepancy may be zero.

4. Discussion

Excellent agreement is obtained between the modulated position of chromium in model *B* and the position determined from $\rho^{\rm MEM}(\mathbf{x}_s)$ in the ordered region ($-0.027 < t < 0.888$) (Fig. 7). Small discrepancies are visible for u_y[Cr], but their magnitudes of up to Δu_y[Cr] = 0.0012 Å are well below the accuracy with which positions of local maxima can be determined for discrete density maps with a mesh of ~ 0.1 Å (van Smaalen *et al.*, 2003). This excellent agreement suggests that the MEM can reliably construct the modulation functions of $Cr_2P_2O_7$. Good agreements between model *B* and the MEM-based modulation functions are also obtained for the atoms O1, O2 and, to a slightly smaller extent, O3.

The modulated position of the P atom does not agree well between $\rho^{\mathbf{MEM}}(\mathbf{x}_s)$ and model *B* (Fig. 7). In particular, the divergence of the modulation functions in model *B* on approaching the disordered regions is unlikely to be a realistic feature of modulations. This interpretation is compounded by the analysis of interatomic distances between P and its four neighboring O atoms, which exhibit very short P—O distances close to the disordered region [Fig. 8(*a*)]. Model *M* is defined such that the modulated atomic positions of phosphorus closely follow the trace of maximum density in $\rho^{\rm MEM}(\mathbf{x}_s)$. The better description of the P atom in model *M* is reflected by the difference-Fourier maps, which exhibit much less structure around the position of P for model *M* than for model *B*, although model *M* retains the larger values of its difference-

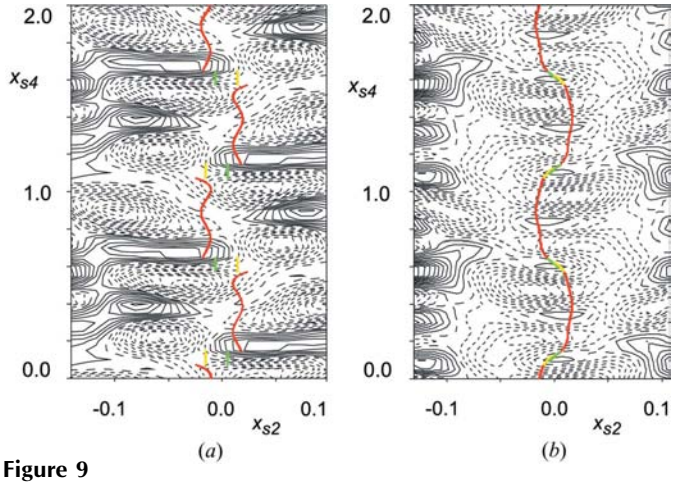

Figure 9
(x_{s2}, x_{s4})-Section of the difference-Fourier map centered at the P atom, and obtained after refinement of (*a*) model *B*, and (*b*) model *M*. Solid lines indicate positive values and dashed lines negative values. The contour interval is 0.02 e Å^{-3}. Minimum and maximum values over the unit cell are $-0.49/0.54$ e Å^{-3} for model *B*, and $-0.47/0.48$ e Å^{-3} for model *M*.

Fourier map at positions farther away from the atoms (Fig. 9). Furthermore, model *M* leads to a shortest P—O distance of 1.46 Å that is longer than the shortest P—O distance of 1.44 Å in model *B*, and compares better to P—O distances of other compounds (Prince, 2006).

Disorder over two sites has already been proposed for the atoms Cr, P, O2 and O3 by Palatinus *et al.* (2006), who gave two positions of half occupancy (model *B*) for each of these atoms. $\rho^{\rm MEM}(\mathbf{x}_s)$ exhibits features that support a split-atom model and allow a refined picture to be developed for the structure within the disordered regions. The MEM densities around the Cr, P and O3 atoms appear to be smeared into the directions of the expected split at those *t* values for which disorder of two sites has been proposed (Figs. 10 and 11). We take this smearing as evidence for the disorder over two sites. It is not a 'smoothing' effect of the MEM, because at most *t* values the maxima of these atoms appear as normal (Figs. 10 and 11). The absence of a double maximum in $\rho^{\rm MEM}(\mathbf{x}_s)$ at the disordered positions is explained by the relatively small distance between the two positions, thus leading to a single broad maximum instead of two peaks, as observed.

The clearest description of the structure in the disordered regions has been obtained for atom O2 [$0.223 < t < 0.306$ for atom O2(i) in Fig. 7]. The MEM density exhibits two closely spaced local maxima near the position of O2 in the *t* sections of the disordered region (Fig. 12). Since both positions are too close to each other for simultaneous occupation, this indicates disorder of the O2 atom over two sites, as they are displayed in Fig. 7, in agreement with model *B* (Palatinus *et al.*, 2006). Unlike model *B*, the positions of O2 within the disordered region depend on *t*.

Analysis of the MEM density allows the unit cell to be dissected into atomic basins (Bader, 1994). The volume of an atomic basin provides a measure for the volume of this atom, while the integrated number of electrons should be equal to the number of electrons carried by this atom in the crystal structure under investigation. For ionic crystals, the integrated number of electrons will deviate from the atomic number, but ionic charges (differences between the atomic numbers and the integrated numbers of electrons) usually cannot be identified with formal valencies. This is especially true if bonding involves a considerable amount of covalency, as is the case for $Cr_2P_2O_7$. For crystals with disorder the integrated atomic charge can thus be taken as a measure for the relative occupancy of each site.

Fig. 13 shows the normalized integrated charge of O2 as a function of the internal coordinate *t*. The number of electrons of O2 is 9.51 within the ordered regions. This number thus corresponds to full occupancy of the O2 site. For the disordered regions it is found that the occupancy of one position gradually increases at the expense of the occupancy of the other position at the same *t* value. The two modulated positions are found to be continuations of the positions in the ordered regions (Fig. 7), whereby – going from the ordered to the disordered regions – the occupancy gradually diminishes (compare Figs. 7 and 13).

These observations led to the following description of the structure of $Cr_2P_2O_7$. The positions of all atoms are modulated, such that the CrO_6 and P_2O_7 units attain different positions and orientations, while deformations of these units lead to internal strain. Strain is released by the existence of disordered positions, which are characterized by the alternate occupancy of one of two conformations/orientations of the CrO_6 and P_2O_7 units. The occupational probability of each site depends on the amount of strain generated by the conformations of these units.

The structure model *M* was developed to capture the various features of the modulation as derived from $\rho^{\rm MEM}(\mathbf{x}_s)$. The observed traces of maximum density provide modulated atomic positions (Fig. 7), while the other density features described above provide information about the structure in the disordered regions. The modulation functions of P were replaced by modulation functions fitted to the traces of maximum density in $\rho^{\rm MEM}(\mathbf{x}_s)$. Furthermore, the distribution of electron density at the P site suggests anharmonic displacements of this atom (Fig. 14). Accordingly, third-order anharmonic ADPs were introduced for the P atom, and their refinement improved the fit to the diffraction data. For the Cr, O1, O2 and O3 atoms the modulation functions of model *B* were kept, because all attempts to introduce MEM-based modulation functions for these atoms led to a fit to the diffraction data that is comparable to model *B*, but worse than model *M*. One explanation for this feature is that $\rho^{\rm MEM}(\mathbf{x}_s)$ and model *B* match very well in the ordered regions, so that model *B* already gives a good description of the ordered regions of

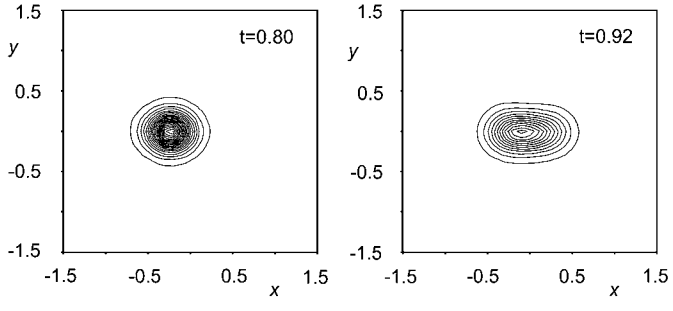

Figure 10
Physical-space sections of the MEM electron density centered at the Cr atom for two values of *t*. The contour interval is 10 e Å^{-3} with a maximum density of 264.82 e Å^{-3}.

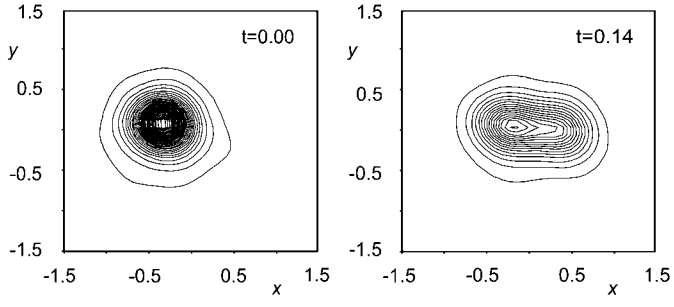

Figure 11
Physical-space sections of the MEM electron density centered at the O3 atom for two values of *t*. The contour interval is 1 e Å^{-3}; the maximum density is 38.2 e Å^{-3}.

the Cr, O1, O2 and O3 atoms. However, the positions derived from the discrete MEM density have an intrinsic uncertainty of ~ 0.01 Å, which might be sufficiently large to provide a less than optimal fit to the diffraction data, while refinement of the many parameters of the MEM-based modulation functions is not possible due to interdependences between them.

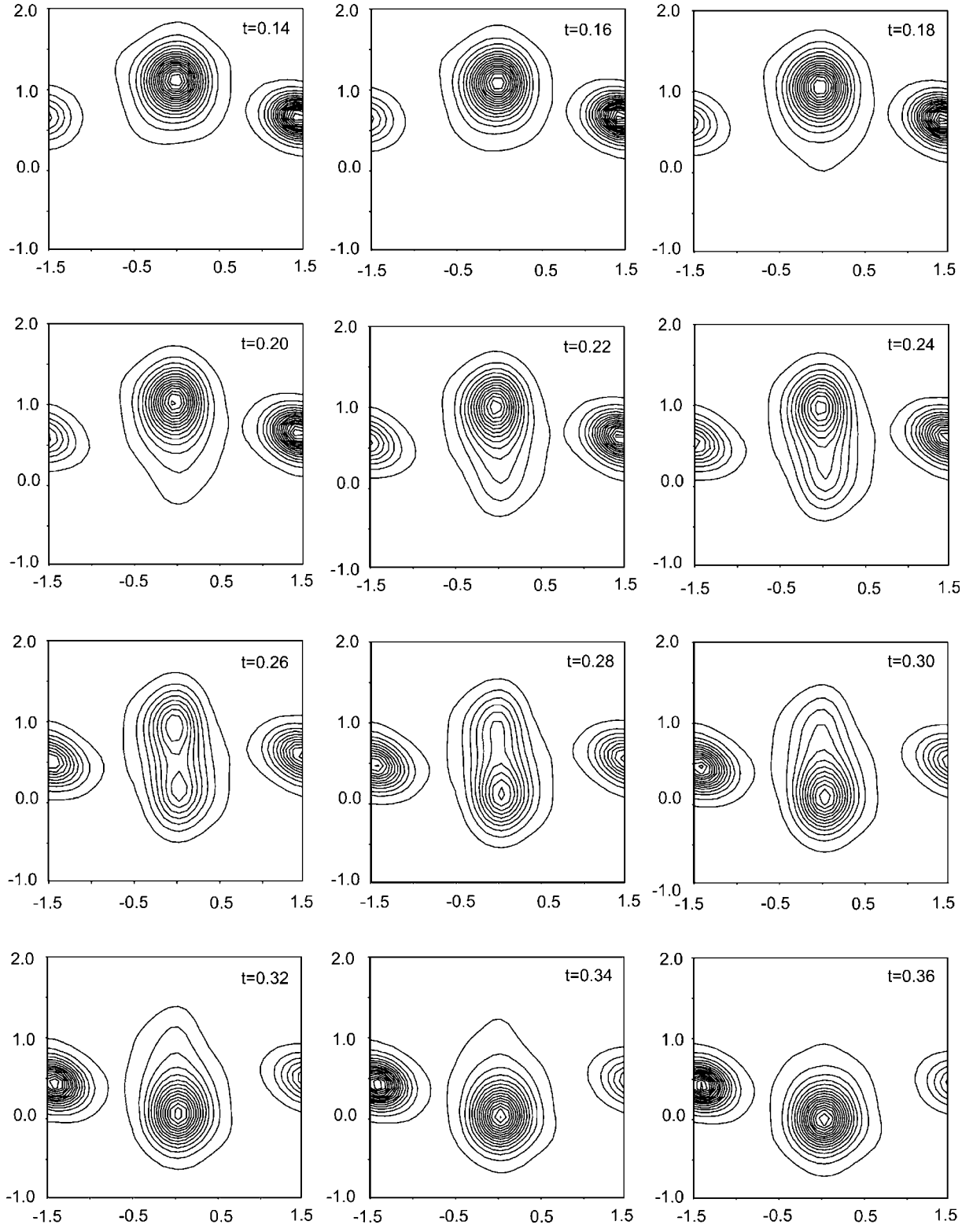

Figure 12
Physical-space sections of the MEM electron density centered at the O2 atom. The value of t is indicated for each section. Axes are labeled in Ångstroms. The contour interval is 1 e Å^{-3}; the maximum density is 29.7 e Å^{-3}. The two partially visible local maxima at the borders of each pane are due to phosphorus atoms.

Modeling the disordered regions is difficult, because we do not have a method to derive split-atom positions from the smeared maxima in $\rho^{\rm MEM}(\mathbf{x}_s)$ in the disordered regions. For the P atom with MEM-based modulation functions, only the basic structure parameters and modulated ADPs have been refined.

Model *M* gives a slightly better fit (R_F = 0.0217) to the diffraction data than model *B* (R_F = 0.0227). Other indicators, *e.g.* the difference-Fourier and Fourier maps around phosphorus (Figs. 9 and 15), also suggest model *M* being the better model. Despite the construction of a complete picture of the modulations in $Cr_2P_2O_7$, it is rather disappointing that this picture could not be translated into a model. This indicates that it is extremely difficult to derive a model for all features of the crystal structure of this compound, which include modulated split-atom disorder but probably also modulated anharmonic ADPs in the disordered regions. Furthermore, the MEM-derived positions cannot be refined due to correlations between parameters, while the accuracy of the MEM-derived positions (∼0.01 Å) is insufficient to give the best possible fit to the diffraction data without further refinement.

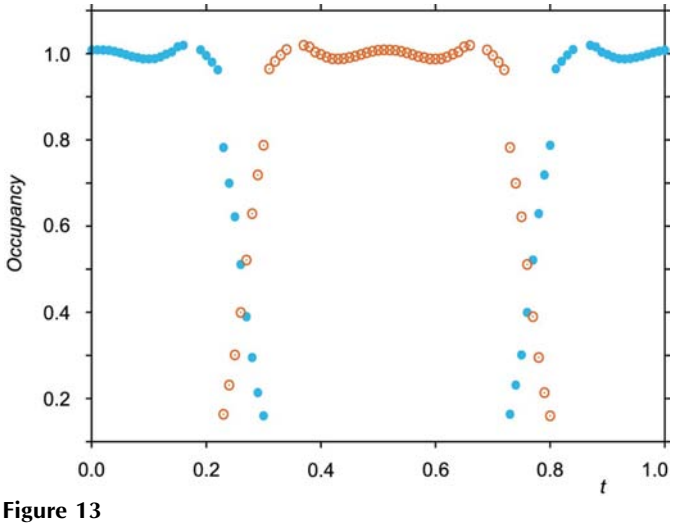

Figure 13
Occupancy of the split-site of atom O2 as a function of *t*. The occupancy is given for O2(i) (open circles; see Fig. 1) and O2(i)* [full circles; symmetry code $(x_1, -x_2, x_3, \frac{1}{2}+x_4)$]. The integrated charge has been normalized against the average integrated charge of 9.51 electrons in the ordered region ($0.32 < t < 0.71$).

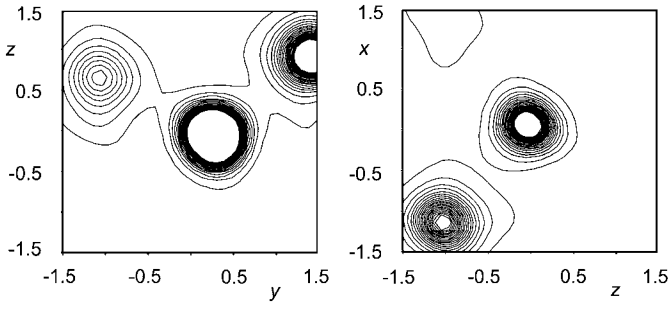

Figure 14
Sections of the MEM electron density parallel to physical space at $t = 0.24$ centered at the P atom. Contours of constant electron density are drawn at intervals of 1 e Å^{-3} up to 20 e Å^{-3}.

5. Conclusions

The Maximum Entropy Method (MEM) in superspace has been applied to X-ray diffraction data of incommensurately modulated $Cr_2P_2O_7$. The interpretation of $\rho^{\rm MEM}(\mathbf{x}_s)$ according to Bader's atoms-in-molecules (AIM) theory has provided the modulated atomic positions, and thus the modulation functions. The modulation functions in the ordered regions of Cr, O1, O2 and O3 have been found to agree well between $\rho^{\rm MEM}(\mathbf{x}_s)$ and model *B* from Palatinus *et al.* (2006).

The MEM has led to a modulation function of phosphorus that is different from model *B* within the ordered regions (Fig. 7). Both the difference-Fourier maps (Fig. 9) and an analysis of P—O interatomic distances (Fig. 8) indicate that the MEM-derived modulation function is closer to the true modulation of phosphorus than the modulation function from model *B*.

The MEM density has provided direct evidence for a split-atom model (Fig. 12), which is interpreted as positions in the structure where the P_2O_7 and CrO_6 groups occur in one of two orientations/conformations with complementary probabilities. Other features derived from $\rho^{\rm MEM}(\mathbf{x}_s)$ are that these probabilities are not equal, but depend on *t*, as well as the fact that the conformations depend on *t*. Furthermore, $\rho^{\rm MEM}(\mathbf{x}_s)$ gives smeared densities of complex shapes around the atoms in the disordered regions, which indicate a structure in the disordered regions that is a combination of modulated positions, modulated occupancies and modulated anharmonic ADPs. We did not succeed in constructing a fully satisfactory structure model that captures all these features.

Reasons for the failure to find a model that would give a much better fit to the diffraction data – especially to the higher-order satellite reflections – than model *B* (Table 4) include the complex nature of the structure, but also the limited accuracy (∼0.01 Å) of MEM-derived positions together with the impossibility of refining all the parameters that

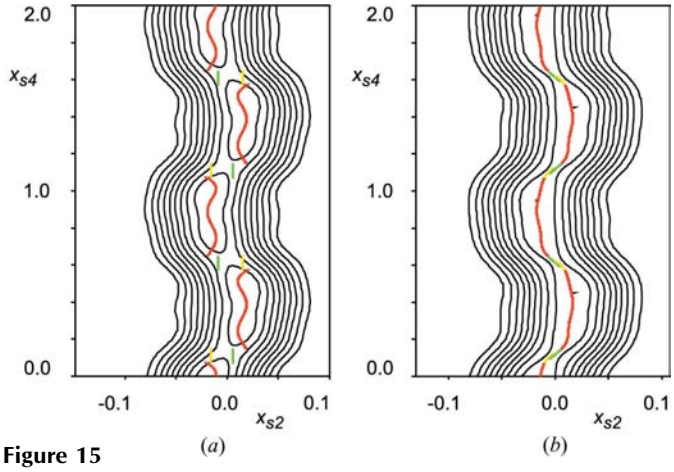

Figure 15
(x_{s2}, x_{s4})-Section of the observed Fourier map of (*a*) model *B*, and (*b*) model *M*. Contours at the intervals of 10% of the maximum density. The modulated position is shown for atoms P (red line), P(*a*) (green line) and P(*b*) (yellow line).

were necessary to construct a model based on $\rho^{\rm MEM}(\mathbf{x}_s)$, owing to interdependences between these parameters. Nevertheless, we believe that the MEM has established the true nature of the modulations in $Cr_2P_2O_7$.

We thank Lukas Palatinus for providing electronic files for the diffraction data and for model *B*, and we thank Vaclav Petricek and Michal Dusek for help with *JANA*2006. Financial support was obtained from the German Science Foundation (DFG).

References

Bader, R. F. W. (1994). *Atoms in Molecules: A Quantum Theory.* Oxford University Press.
Bagautdinov, B., Luedecke, J., Schneider, M. & van Smaalen, S. (1998). *Acta Cryst.* B**54**, 626–634.
Dinnebier, R. E., Schneider, M., van Smaalen, S., Olbrich, F. & Behrens, U. (1999). *Acta Cryst.* B**55**, 35–44.
Gilmore, C. J. (1996). *Acta Cryst.* A**52**, 561–589.
Glaum, R., Walter-Peter, M., Oezalp, D. & Gruehn, R. (1991). *Z. Anorg. Allg. Chem.* **601**, 145–162.
Hofmann, A., Netzel, J. & van Smaalen, S. (2007). *Acta Cryst.* B**63**, 285–295.
Janssen, T., Chapuis, G. & de Boissieu, M. (2007). *Aperiodic Crystals. From Modulated Phases to Quasicrystals.* Oxford University Press.
Kumazawa, S., Takata, M. & Sakata, M. (1995). *Acta Cryst.* A**51**, 651–658.
McMahon, M. I., Degtyareva, O., Nelmes, R. J., van Smaalen, S. & Palatinus, L. (2007). *Phys. Rev. B*, **75**, 184114.
Netzel, J., Hofmann, A. & van Smaalen, S. (2008). *CrystEngComm*, **10**, 335–343.
Palatinus, L., Dušek, M., Glaum, R. & El Bali, B. (2006). *Acta Cryst.* B**62**, 556–566.
Palatinus, L. & van Smaalen, S. (2002). *Acta Cryst.* A**58**, 559–567.
Palatinus, L. & van Smaalen, S. (2004). *Z. Kristallogr.* **219**, 719–729.
Petricek, V., Dušek, M. & Palatinus, L. (2006). *JANA*2006. Institute of Physics, Praha, Czech Republic.
Prince, E. (2006). Editor. *International Tables for Crystallography*, Vol. C. Dordrecht: Kluwer Academic Publishers.
Sakata, M. & Sato, M. (1990). *Acta Cryst.* A**46**, 263–270.
Takata, M. (2008). *Acta Cryst.* A**64**, 232–245.
van Smaalen, S. (2007). *Incommensurate Crystallography.* Oxford University Press.
van Smaalen, S. & Li, L. (2009). *Phys. Scr.* **79**, 048305.
van Smaalen, S. & Netzel, J. (2009). *Phys. Scr.* **79**, 048304.
van Smaalen, S., Palatinus, L. & Schneider, M. (2003). *Acta Cryst.* A**59**, 459–469.
Vries, R. Y. de, Briels, W. J. & Feil, D. (1994). *Acta Cryst.* A**50**, 383–391.
Wang, C.-R., Kai, T., Tomiyama, T., Yoshida, T., Kobayashi, Y., Nishibori, E., Takata, M., Sakata, M. & Shinohara, H. (2001). *Angew. Chem. Int. Ed.* **40**, 397–399.
Yamamoto, A., Weber, S., Sato, A., Kato, K., Ohshima, K., Tsai, A. P., Niikura, A., Hiraga, K., Inoue, A. & Masumoto, T. (1996). *Philos. Mag. Lett.* **73**, 247-254.